

Contents lists available at ScienceDirect

Journal of Energy Chemistry

http://www.journals.elsevier.com/

journal homepage: www.elsevier.com/locate/jechem

Achieving photocatalytic water oxidation on LaNbON₂ under visible light irradiation

Lipeng Wan a,b, Feng-Qiang Xiong a,*, Bingxue Zhang C, Ruxin Che b, Yue Li a,b, Minghui Yang a,c,*

- ^a Dalian National Laboratory for Clean Energy, Dalian Institute of Chemical Physics, Chinese Academy of Sciences, Dalian 116023, Liaoning, China
- ^b College of Materials Science and Engineering, College of Environmental and Chemical Engineering, Dalian Jiaotong University, Dalian 116028, Liaoning, China
- ^c Ningbo Institute of Material Technology and Engineering, Chinese Academy of Sciences, Ningbo 315201, Zhejiang, China

ARTICLE INFO

Article history: Received 16 October 2017 Revised 7 January 2018 Accepted 9 January 2018

Keywords:
Photocatalysis
Perovskite oxynitride
Water splitting
Anion vacancy
Valence band

ABSTRACT

LaNbON $_2$ has narrow bandgap and wide visible-light absorption band, yet no photocatalytic water oxidation on LaNbON $_2$ has been reported. By a post-annealing treatment in Ar, anion vacancies were brought into LaNbON $_2$ as shown by EPR spectroscopy. These could act as donors in the semiconductor. And consequently the oxidative power of holes was enhanced as indicated by the difference between fermi level and valence band maximum (E_F - E_{VBM}) evaluated from valence band XPS. The annealed LaNbON $_2$ photocatalyst acquired water oxidation ability for the first time, which was improved by combining CoO_x as cocatalyst. Annealed LaNbON $_2$ derived from La $_3$ NbO $_7$ had smaller particle size, higher concentration of anion vacancies, bigger E_F - E_{VBM} and better performance for photocatalytic oxygen evolution reaction than LaNbON $_2$ derived from LaNbO $_4$.

© 2018 Science Press and Dalian Institute of Chemical Physics, Chinese Academy of Sciences. Published by Elsevier B.V. and Science Press. All rights reserved.

1. Introduction

Several niobium oxynitride perovskites are promising candidate semiconductors for solar energy conversion owing to their wide visible light absorption [1,2]. Water oxidation and hydrogen production reactions have been reported using these photocatalysts, including CaNbO₂N ($\lambda_{max} \sim 600$ nm), SrNbO₂N ($\lambda_{max} \sim 690$ nm) and BaNbO₂N ($\lambda_{max} \sim 740$ nm), in the forms of both powder suspension [1,3,4] and photoanode [2,5]. This shows their potential in solar fuel production from water splitting. The lanthanum analogue LaNbON₂ has a bandgap ~ 1.65 eV, corresponding to absorption band edge around 750 nm [1,6], which can absorb most parts of visible light. Calculating from the air mass 1.5 solar spectral irradiance, if the absorbed photons are utilized for photocatalytic water splitting, the theoretical limit of the solar-to-hydrogen efficiency is $\sim 29\%$ for the LaNbON₂ photocatalyst (see supplementary information).

On the other hand, the bandgap of $LaNbON_2$ is only about 0.42 eV bigger than the thermodynamic energy for water splitting, thus total driving force is very limited compared to the

E-mail addresses: fqxiong@dicp.ac.cn (F.-Q. Xiong), myang@dicp.ac.cn (M. Yang).

overpotentials for water oxidation and hydrogen evolution. Several factors need to be well engineered for the stages of photocatalysis process in order to ensure effective performance of photocatalysts. The factors include (i) carrier lifetime withstanding recombination, (ii) energy loss during charge separation and (iii) driving force (determined by band positions) and overpotentials for surface reaction. These make great challenges for the material design and optimization. As a result, only one example of hydrogen evolution on LaNbON2 has been reported so far using CH3OH as a sacrificial reagent [7]. However, no achievement for water oxidation on this material has been reported yet. In the water oxidation reaction, transfer of 4-photogenerated holes and formation of O-O bond are involved for evolving per O2. These make a complex process. Significant driving force is required to overcome the energy barrier [8]. Meanwhile, the process is challenged by electron-hole recombination unless the carriers are well separated [9]. These make photocatalytic water oxidation difficult for LaNbON2 with a relatively narrow bandgap.

In this work, we point out an aspect of engineering $LaNbON_2$ for photocatalytic water oxidation. It was observed that $LaNbON_2$ samples prepared via thermal ammonolysis of $LaNbO_4$ (labeled as $LaNbON_2$ -f.114) and La_3NbO_7 (labeled as $LaNbON_2$ -f.317) were not active for photocatalytic water oxidation. In order to adjust semiconductor properties, $LaNbON_2$ -f.114 and $LaNbON_2$ -f.317 were

^{*} Corresponding authors.

annealed at 700 °C in an inert atmosphere (labeled as LaNbON₂-f.114-Ar700 and LaNbON₂-f.317-Ar700). The annealing treatment resulted into anion vacancies in the samples, which in turn acted as electron-donors in the as-prepared LaNbON₂ semiconductor. The difference between fermi level and valence band maximum ($E_{\rm F}$ - $E_{\rm VBM}$) was increased from ~1.0 eV to ~1.2 eV for LaNbON₂-f.114-Ar700 and from ~0.9 eV to ~1.5 eV for LaNbON₂-f.317-Ar700 after the annealing treatment. This in turn increased the oxidative power of the photogenerated holes in LaNbON₂. The annealed LaNbON₂ with anion vacancies exhibited enhanced performance of photocatalytic water oxidation, which was further improved using CoO_x as cocatalyst.

2. Experimental

2.1. Preparation of LaNbON₂ samples

Firstly, LaNbON₂ was prepared via nitridation of metal oxide precursor following the procedures in previous work [10]. In brief, the precursors LaNbO₄ and La₃NbO₇ were synthesized from the reactions of stoichiometric La₂O₃ and Nb₂O₅ (Sinopharm Chemical, 99.99%) at 1000 °C for 5 h using NaCl and KCl (Aladdin, 99.99%) as flux. And then LaNbON₂-f.114 was prepared via nitridation of LaNbO₄ under an NH₃ flow (99.999%) of 250 sccm at 950 °C for 15 h. LaNbON₂-f.317 was prepared via Nitridation of La₃NbO₇ using the same procedure, followed by removal of La₂O₃ by washing with diluted H₂SO₄. Secondly, LaNbON₂ was annealed in Ar at 700 °C for 15 min, followed by a natural cooling.

2.2. Loading of cocatalysts

 CoO_x , an efficient cocatalyst for water oxidation on (oxy)nitride semiconductors, was loaded via an impregnation method [4,11–13]. A calculated amount (2 wt% Co) of $CoCl_2$ aqueous solution was impregnated on the surface of $LaNbON_2$ in a heated water-bath. The as-impregnated powder was heated at 700 °C for 1 h and naturally cooled under an NH_3 flow of 200 sccm. The obtained sample was further annealed in air at 200 °C for 1 h to convert the metallic cobalt into the oxide form.

2.3. Characterizations

The crystal structure was characterized using X-ray diffraction (XRD, Rigaku Miniflex 600 X-ray diffractometer, Cu Kα; accelerating voltage, 40 kV; applied current, 15 mA; scanning rate, 5 °/min). The morphology was examined by scanning electron microscopy (SEM, JSM-7800F, Japan). Electron paramagnetic resonance (EPR) was recorded at 104K (Brucker EPR A200 spectrometer, center field, 3450 G; microwave frequency, 9.32 GHz). Mott-Schottky analysis was carried out in a 0.5 M Na₂SO₄ with addition of La₂O₃ (undissolved, 0.2 g L⁻¹, pH 8.8) on a potentiostat (CHI660E, frequency, 1 kHz). The working electrode was LaNbON2 particles on Al substrate, and Pt and SCE were used as counter and reference electrodes, respectively. The potentials were converted to the reversible hydrogen electrode (RHE) scale. UV-Vis diffuse reflectance spectra were recorded on a spectrophotometer (Hitachi U-3900 spectrometer) using a BaSO₄ standard as the reference. The valence band (VB) X-ray photoelectron spectra (XPS) were obtained on an ESCALAB250Xi (using Al $K\alpha$, 1486.6 eV) using contamination C1s (284.8 eV) for the calibration.

2.4. Photocatalytic water oxidation

The photocatalytic performance for water oxidation was tested in a quartz-covered Pyrex vessel connected to a gas chromatograph

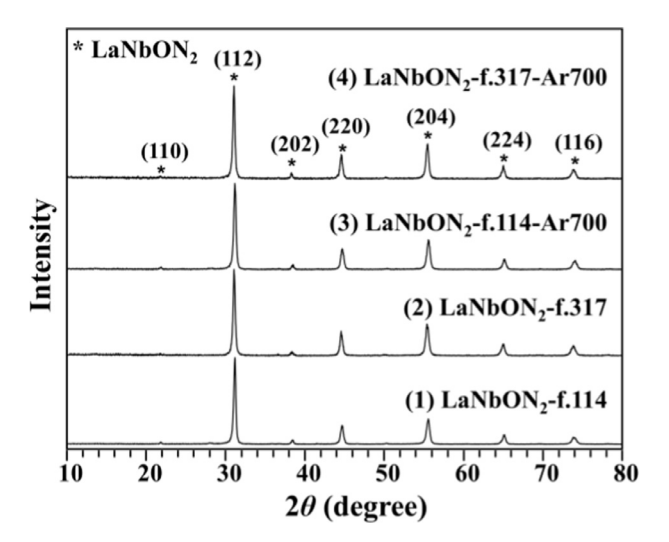


Fig. 1. XRD patterns of (1) LaNbON₂-f.114, (2) LaNbON₂-f.317, (3) LaNbON₂-f.114-Ar700 and (4) LaNbON₂-f.317-Ar700.

(GC), which was equipped with a vacuum line. The reactant solution was comprised of water, photocatalyst, AgNO $_3$ and La $_2$ O $_3$. AgNO $_3$ and La $_2$ O $_3$ were electron acceptor reagent and pH buffer, respectively, which are commonly used in water oxidation using (oxy)nitride photocatalysts [1,11,12]. The temperature was maintained using a flow of cooling water at 10 °C. The reaction vessel was evacuated to ensure that air is completely removed, then irradiated from the topside for 0.5 h, using a 300 W xenon lamp with a filtration mirror ($\lambda \geq 400\,\mathrm{nm}$). This mirror cuts off the ultraviolet light. And the evolved gases were analyzed by online GC using Ar as carrier gas, and divided by the weight of photocatalyst and the time for normalization.

3. Results and discussion

LaNbON₂-f.114 and LaNbON₂-f.317 were prepared following the procedures in previous work [10]. As shown in Fig. 1(1) and (2), perovskite-type LaNbON2 samples were obtained via nitridation of LaNbO₄ and La₃NbO₇, respectively. This was followed by acid treatment to remove by-product La₂O₃. It has been reported that perovskite-type oxynitrides like SrNbO2N and LaTiO2N are not thermodynamically stable at high temperature in inert atmosphere, which cause visible weight loss starting from ~850 °C and forming low-valent nitride phase in the final products during thermogravimetric analysis [14]. Nevertheless, the LaNbON₂ samples retained perovskite phase after annealing in Ar at a lower temperature 700 °C (Fig. 1(3), LaNbON₂-f.114-Ar700 and Fig. 1(4), LaNbON₂f.317-Ar700). SEM images of LaNbON₂ samples are shown in Fig. 2. The particle sizes of LaNbON2 samples derived from La3NbO7 were smaller than those derived from LaNbO₄, as a result of the formation and subsequent removal of by-product La₂O₃ during preparation. And the particle sizes of annealed LaNbON₂ samples were similar to the respective untreated ones, except for the fact that the thin connection among LaNbON2 particles was cracked after the annealing treatment. Specifically, the particles were approximately 100 nm for LaNbON₂-f.114-Ar700, and 30 nm for LaNbON₂f.317-Ar700.

The generation of anion vacancies during the annealing treatment was examined via EPR spectroscopy. As shown in Fig. 3, no resolvable signals were observed in the LaNbON₂-f.114 and LaNbON₂-f.317 samples. In contrast, the annealed LaNbON₂ samples showed significant EPR signals around g-value of 2.004, which is attributed to anion vacancies [15–17]. And the intensity for LaNbON₂-f.317-Ar700 was much stronger than that for LaNbON₂-

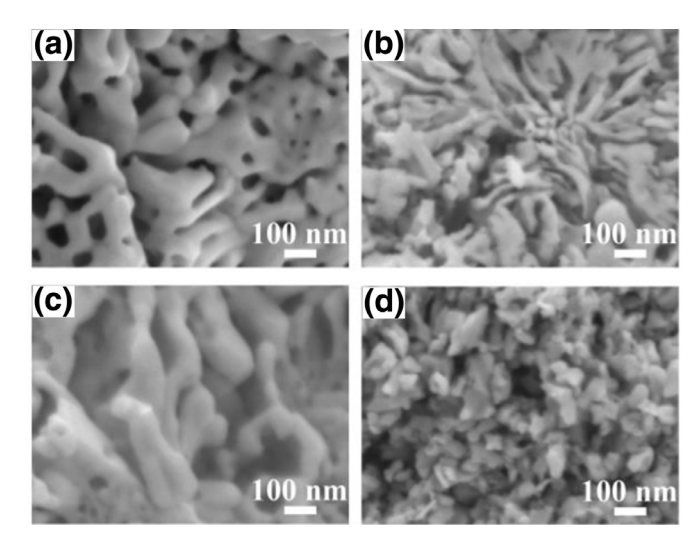


Fig. 2. SEM images of (a) LaNbON₂-f.114, (b) LaNbON₂-f.317, (c) LaNbON₂-f.114-Ar700 and (d) LaNbON₂-f.317-Ar700.

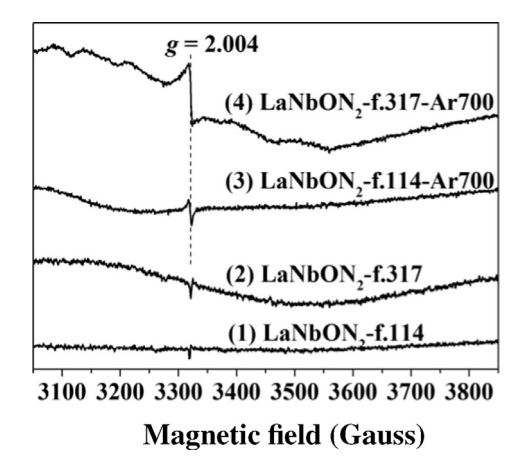


Fig. 3. EPR spectra of (1) LaNbON $_2$ -f.114, (2) LaNbON $_2$ -f.317, (3) LaNbON $_2$ -f.114-Ar700 and (4) LaNbON $_2$ -f.317-Ar700.

f.114-Ar700. It is revealed that anion vacancies arouse from the annealing treatment at 700 °C. Interestingly, the annealing temperature and duration was moderate, avoiding the destruction of the perovskite-type crystal structure. LaNbON $_2$ -f.317-Ar700 exhibited more anion vacancies than LaNbON $_2$ -f.114-Ar700 after the annealing treatment, probably owing to its smaller particle size and higher surface area. The anion vacancies, including nitrogen vacancy ($\rm V_N$) and oxygen vacancy ($\rm V_O$) in the LaNbON $_2$ crystal lattice could be thermally ionized as below,

$$V_N \rightleftharpoons V_N^{\cdot} + e^{\prime} \rightleftharpoons V_N^{\cdot \cdot} + 2e^{\prime} \rightleftharpoons V_N^{\cdot \cdot \cdot} + 3e^{\prime} \tag{1}$$

$$V_0 \rightleftharpoons V_0' + e' \rightleftharpoons V_0'' + 2e' \tag{2}$$

and act as donors giving electrons to the conduction band of LaNbON₂. The change in donor concentration was estimated via Mott–Schottky analysis. As shown in Fig. 4, positive slopes of Mott–Schottky curves revealed n-type character of the LaNbON₂ samples. Moreover, the slope for LaNbON₂-f.317-Ar700 was much lower than that of LaNbON₂-f.317. According to the Mott–Schottky equation [18], this indicates that the donor concentration of LaNbON₂-f.317-Ar700 was much higher than that of LaNbON₂-f.317

As shown by UV–Vis diffuse reflectance spectra (DRS) in Fig. 5, the absorption band edges of LaNbON $_2$ -f.317 and LaNbON $_2$ -f.114 were similar (\sim 750 nm), which correspond to the band gap of

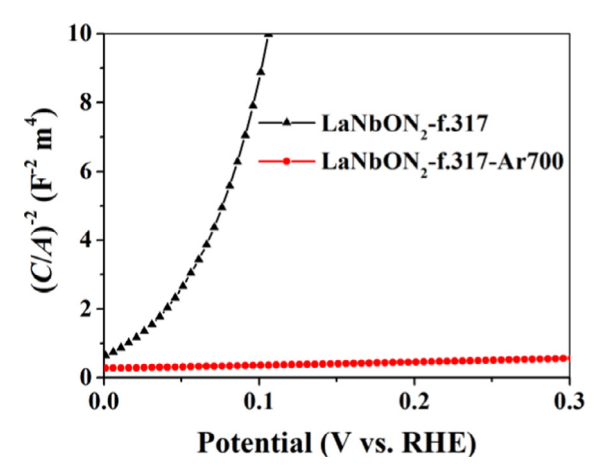


Fig. 4. Mott-Schottky plots of $LaNbON_2$ -f.317 and $LaNbON_2$ -f.317-Ar700 on Al substrates

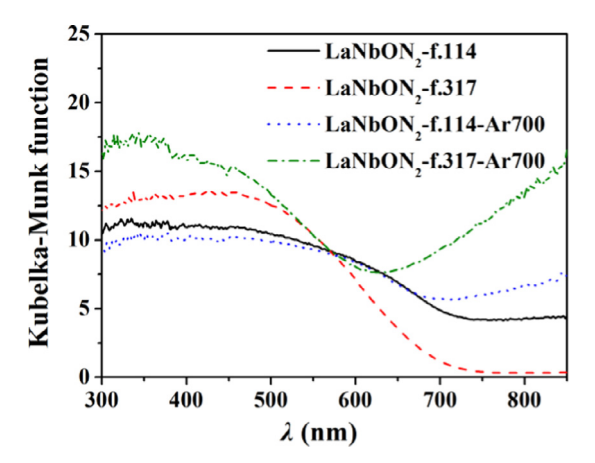


Fig. 5. UV–Vis DRS of LaNbON $_2$ -f.114, LaNbON $_2$ -f.317, LaNbON $_2$ -f.114-Ar700 and LaNbON $_2$ -f.317-Ar700.

1.65 eV. However, beyond the band edge wavelength, LaNbON₂f.114 had obvious absorption while LaNbON₂-f.317 exhibited rather slight defect absorption [10]. The absorption beyond the band edge wavelength arose after annealing treatment for LaNbON2-f.317-Ar700, which sweeps up to the end of the UV-Vis spectrum. It was difficult to precisely determine the band absorption edge, because the band absorption overlapped with an upswept defect absorption feature rather than a flat defect absorption feature. Roughly, the absorption edges were evaluated via deducting the defect absorption (Fig. S1), which were about 740 and 700 nm for LaNbON₂f.114-Ar700 and LaNbON2-f.317-Ar700, respectively. The blue-shift in absorption band edge could arise from Burstein-Moss effect due to high density of electrons that result from anion vacancies acting as donors in the n-type semiconductor [19,20]. The bigger blueshift for LaNbON₂-f.317-Ar700 than that for LaNbON₂-f.114-Ar700 was consistent with the higher concentration of anion vacancies shown by EPR spectroscopy.

Moreover, the presence of the high concentration of donors had an effect on the fermi level of the LaNbON $_2$ semiconductor. The valence band X-ray photoelectron spectroscopy (VB-XPS) was investigated to determine E_F - E_{VBM} (i.e. binding energy of VB edge) near the surface. As shown in Fig. 6, E_F - E_{VBM} for LaNbON $_2$ -f.114 and LaNbON $_2$ -f.317 were similar, about 1.0 eV and 0.9 eV, respectively. Interestingly, E_F - E_{VBM} increased after the annealing treatment. The values were 1.2 eV and 1.5 eV for LaNbON $_2$ -f.114-Ar700 and LaNbON $_2$ -f.317-Ar700, respectively. The fermi level could be elevated by increasing the concentration of donors, which was

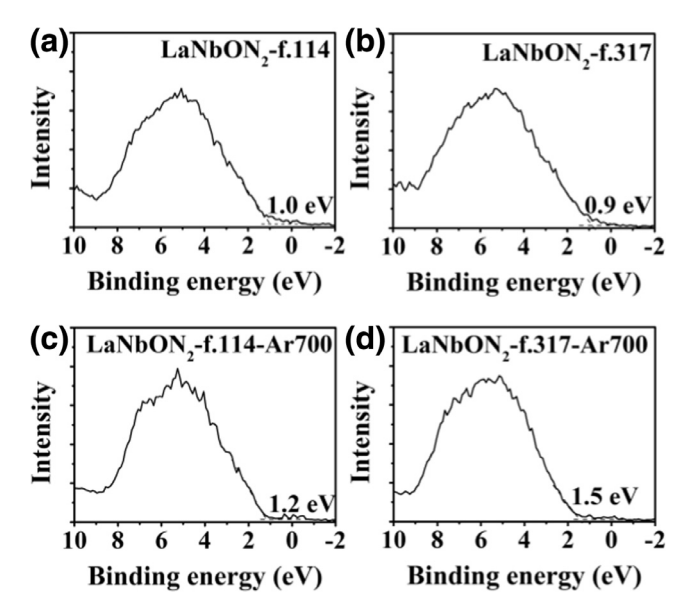


Fig. 6. VB-XPS of (a) LaNbON $_2$ -f.114, (b) LaNbON $_2$ -f.317, (c) LaNbON $_2$ -f.114-Ar700 and (d) LaNbON $_2$ -f.317-Ar700.

Table 1. Oxygen evolution on LaNbON2 photocatalysts under visible light irradiation from a Xe lamp ($\lambda \ge 400\,\text{nm}$).

Photocatalyst	Oxygen evolution (μmol h ⁻¹ g ⁻¹)
LaNbON ₂ -f.114	below quantification limit
LaNbON ₂ -f.317	below quantification limit
CoO _x /LaNbON ₂ -f.114	below quantification limit
CoO _x /LaNbON ₂ -f.317	below quantification limit
LaNbON ₂ -f.114-Ar700	below quantification limit
LaNbON ₂ -f.317-Ar700	33
CoO _x /LaNbON ₂ -f.114-Ar700	5
$CoO_x/LaNbON_2$ -f.317-Ar700	108

Photocatalyst, 0.05 g LaNbON $_2$ with/without cocatalyst; pH buffer, 0.1 g La $_2$ O $_3$; reaction solution, 100 mL 10 mM aqueous AgNO $_3$ solution, 10 °C.

consistent with the results of the UV–Vis DRS and EPR spectroscopy. The increase in $E_{\rm F}$ – $E_{\rm VBM}$ would enhance the oxidative power of the photogenerated holes in LaNbON $_2$.

The photocatalytic performance of LaNbON2 photocatalysts for water oxidation was tested under visible light irradiation using AgNO₃ as electron scavenger, which is shown in Table 1. In order to improve the photocatalytic performance, CoO_x cocatalyst was loaded on LaNbON2 via an impregnation method. In line with previous report [1], no activity was found on the conventional LaNbON₂-f.114. The photocatalytic performance of LaNbON₂-f.317 would be expected to be better than LaNbON2-f.114 in view of the smaller particle size and the decrease in defect-promoted recombination, but LaNbON₂-f.317 gave no detectable photocatalytic oxygen evolution. This result was similar to low performance of low-defect LaTiO₂N prepared from La₂TiO₅, which could be attributed to inefficient built-in electric field and insufficient oxidative power of photogenerated holes [13]. Even after loading CoO_x as cocatalyst for water oxidation, no photocatalytic oxygen evolution was detected on either LaNbON₂-f.114 or LaNbON₂-f.317. Interestingly, after the annealing treatment, LaNbON₂-f.317-Ar700 achieved a performance for photocatalytic oxygen evolution (33 μ mol h⁻¹ g⁻¹), though LaNbON₂-f.114-Ar700 gave no detectable photocatalytic oxygen evolution. The combination of CoO_x cocatalyst led to significant increase in the oxygen evolution, estimated to be 5 μ mol h^{-1} g^{-1} for $CoO_x/LaNbON_2$ -f.114-Ar700 photocatalyst. And it was further improved to 108 μmol h⁻¹ g⁻¹ for CoO_x/LaNbON₂-f.317-Ar700 photocatalyst.

Anion vacancies in the annealed LaNbON₂ photocatalysts revealed by EPR could act as donors in the semiconductor and promote charge separation of photogenerated electrons and holes [13,21]. Furthermore, the $E_{\rm F}$ - $E_{\rm VBM}$ was increased from \sim 1.0 eV to \sim 1.2 eV in LaNbON₂-f.114-Ar700 and from \sim 0.9 eV to \sim 1.5 eV in LaNbON₂-f.317-Ar700. This significantly increased the oxidative power of the photogenerated holes in LaNbON2 when the semiconductor came in contact with aqueous solution and formed semiconductor-liquid junction, so that water oxidation reaction took place on the annealed LaNbON2 photocatalysts in particular LaNbON₂-f.317-Ar700. The anion vacancies were generated by the annealing treatment, which would diffuse into the bulk at the high temperature. As shown by EPR spectroscopy, the anion vacancies (g=2.004) remained in LaNbON₂ after photocatalytic water oxidation (Fig. S2). This indicates the good stability of anion vacancies during photocatalysis. Compared to LaNbON2-f.114-Ar700, besides the significant effects of higher concentration of anion vacancies, the paths to the surface for photogenerated electrons and holes in LaNbON2-f.317-Ar700 were shorter, which could also contribute to the better performance of LaNbON2-f.317-Ar700 photocatalysts than LaNbON₂-f.114-Ar700 photocatalysts.

4. Conclusions

In summary, water oxidation was achieved using LaNbON $_2$ photocatalysts under visible light irradiation, which reveals the possibility of LaNbON $_2$ for the application of solar water splitting. By a simple annealing treatment of LaNbON $_2$ derived from LaNbO $_4$ and La $_3$ NbO $_7$, the material was engineered with anion vacancies which act as donors in the semiconductor. The consequent big $E_{\rm F}E_{\rm VBM}$ promoted the surface reaction of water oxidation. This result could be illuminating for engineering narrow bandgap semiconductor photocatalysts to improve water oxidation performance.

Acknowledgments

This work was supported by the National Natural Science Foundation of China (no. 21503220 and 21471147), and the Natural Science Foundation of Liaoning Province (no. 201501045). M. Yang would like to thank the Thousand Youth Talents Plan of China.

Supplementary materials

Supplementary material associated with this article can be found, in the online version, at doi:10.1016/j.jechem.2018.01.004.

References

- [1] B. Siritanaratkul, K. Maeda, T. Hisatomi, K. Domen, ChemSusChem 4 (2011) 74–78.
- [2] J. Seo, Y. Moriya, M. Kodera, T. Hisatomi, T. Minegishi, M. Katayama, K. Domen, Chem. Mater. 28 (2016) 6869–6876.
- [3] J.Q. Wang, X. Wang, B. Liu, X.H. Li, M.H. Cao, Mater. Lett. 152 (2015) 131-134.
- [4] T. Hisatomi, C. Katayama, Y. Moriya, T. Minegishi, M. Katayama, H. Nishiyama, T. Yamada, K. Domen, Energy Environ. Sci. 6 (2013) 3595–3599.
- [5] H. Urabe, T. Hisatomi, T. Minegishi, J. Kubota, K. Domen, Faraday Discuss. 176 (2014) 213–223.
- [6] D. Logvinovich, S.G. Ebbinghaus, A. Reller, I. Marozau, D. Ferri, A. Weidenkaff, Z. Anorg, Allg. Chem. 636 (2010) 905–912.
- [7] C. Izawa, T. Kobayashi, K. Kishida, T. Watanabe, Adv. Mater. Sci. Eng. 2014 (2014) 465720.
- [8] M.M. Waegele, X.H. Chen, D.M. Herhihy, T. Cuk, J. Am. Chem. Soc. 136 (2014) 10632–10639.
- [9] F. Le Formal, S.R. Pendlebury, M. Cornuz, S.D. Tilley, M. Gratzel, J.R. Durrant, J. Am. Chem. Soc. 136 (2014) 2564–2574.
- [10] L. Wan, F.-Q. Xiong, Y. Li, T. Thomas, R. Che, M. Yang, Mater. Lett. 188 (2017) 212–214.
- [11] F. Zhang, A. Yamakata, K. Maeda, Y. Moriya, T. Takata, J. Kubota, K. Teshima, S. Oishi, K. Domen, J. Am. Chem. Soc. 134 (2012) 8348–8351.
- [12] S. Chen, S. Shen, G. Liu, Y. Qi, F. Zhang, C. Li, Angew. Chem. Int. Ed. 54 (2015) 3047–3051.

- [13] F.Q. Xiong, L. Wan, Y. Li, T. Thomas, F.J. DiSalvo, M. Yang, ChemSusChem 10 (2017) 930–937.
- [14] R. Aguiar, D. Logvinovich, A. Weidenkaff, A. Reller, S.G. Ebbinghaus, Thermochim. Acta 471 (2008) 55–60.
 [15] D.A. Popescu, J.M. Herrmann, A. Ensuque, F. Bozon-Verduraz, Phys. Chem.
- Chem. Phys. 3 (2001) 2522–2530. [16] S.L. Zhang, W. Li, Z.S. Jin, J.J. Yang, J.W. Zhang, Z.L. Du, Z.J. Zhang, J. Solid State Chem. 177 (2004) 1365–1371.
- [17] T.R. Gordon, M. Cargnello, T. Paik, F. Mangolini, R.T. Weber, P. Fornasiero, C.B. Murray, J. Am. Chem. Soc. 134 (2012) 6751–6761.

 [18] R. Krishnan, Encyclopedia of Electrochemistry, Wiley-VCH Verlag GmbH & Co.
- KGaA, 2007.
- [19] Q. Wang, M. Brier, S. Joshi, A. Puntambekar, V. Chakrapani, Phys. Rev. B 94 (2016) 245305.
- [20] V.Y. Davydov, A.A. Klochikhin, Semiconductors 38 (2004) 861–898.
- [21] G.M. Wang, H.Y. Wang, Y.C. Ling, Y.C. Tang, X.Y. Yang, R.C. Fitzmorris, C.C. Wang, J.Z. Zhang, Y. Li, Nano Lett. 11 (2011) 3026–3033.